Research Square

Preprints are preliminary reports that have not undergone peer review.
They should not be considered conclusive, used to inform clinical practice,
or referenced by the media as validated information.

An Analytical Feasibility Boundary Reveals A Near-Threshold Identifiability Limit for Externally Transmitted Confinement in Closed Mitosis

Hyeonje Yang

yanghj0206@snu.ac.kr

Seoul National University https://orcid.org/0009-0007-5151-0528

Research Article

Keywords: Closed mitosis, nuclear envelope mechanics, mitotic spindle, mechanical confinement, spindle buckling

Posted Date: November 20th, 2026

DOI: https://doi.org/10.21203/rs.3.rs-10885507/v2

License: This work is licensed under a Creative Commons Attribution 4.0 International License.
Read Full License

Additional Declarations: The authors declare no competing interests.

An Analytical Feasibility Boundary Reveals a Near-Threshold Identifiability Limit for Externally Transmitted Confinement in Closed Mitosis

Hyeonje Yang

Department of Biological Sciences, Seoul National University, Seoul, Republic of Korea

Corresponding author: yanghj0206@snu.ac.kr

ORCID: 0009-0007-5151-0528

[1*]Hyeonje Yang

[1]Department of Biological Sciences, Seoul National University, Seoul, Republic of Korea

[*]:corresponding author: yanghj0206@snu.ac.kr

ORCID: 0009-0007-5151-0528

Abstract

Closed mitosis mechanically couples an elongated spindle to a deformable nuclear envelope (NE), but it is unclear when mechanical confinement outside the cell could become relevant to this intranuclear force balance. I formulate a deliberately reduced problem: an externally imposed confinement pressure p_{confine} is transmitted to the NE with an unknown fraction T, producing an effective load $p_{\mathrm{eff}} = T\, p_{\mathrm{confine}}$. Combining established membrane-tether mechanics with an adopted spindle-force threshold F_b, I derive an exact dimensionless feasibility boundary. With $f_0 = 2\pi\sqrt{2\kappa\sigma}$, $\mu = \frac{F_b}{f_0}$, and $\chi = Tp_{\mathrm{confine}}\sqrt{\frac{\kappa}{2\sigma^3}}$, threshold compatibility for $\mu \geq 1$ is $\chi \geq q^*(\mu)$, where $q^*(\mu)$ is available in closed form. The boundary is strictly increasing and convex. Its exact logarithmic sensitivities diverge as $\mu \to 1^+$, making numerical thresholds intrinsically ill-conditioned near the $\mu = 1$ boundary. Using Lim et al.'s fitted membrane ratio with their adopted effective bending rigidity ($\kappa = 400pN\ nm$, $\sigma = 0.026\frac{\mathrm{pN}}{\mathrm{nm}}$) together with an illustrative $F_b = 31pN$ gives $\mu \approx 1.082$ and $p^* \approx 113\ Pa$. However, the local elasticity with respect to F_b is approximately 15.1. Thus, the numerical pressure is not a robust biological prediction. Instead, the analysis identifies a near-boundary calibration and identifiability limitation. Scenario propagation shows frequent switching into the $\mu \leq 1$ regime under modest parameter perturbations, especially when the fitted membrane ratio is preserved. Spindle-force calibration and external-to-NE load transmission must be measured before confinement can be assigned a quantitative role in closed mitosis.

Keywords: Closed mitosis; nuclear envelope mechanics; mitotic spindle; mechanical confinement; spindle buckling

1. Introduction

Eukaryotes span a spectrum of mitotic strategies rather than a strict open/closed binary[1, 2]. In the fission yeast *Schizosaccharomyces pombe* (*S. pombe*), spindle assembly and chromosome segregation occur predominantly within a nuclear compartment that remains intact through most of mitosis, although late nuclear division requires localized remodeling and disassembly of the NE[3]. This geometry creates an unusual mechanical problem: the anaphase spindle elongates while physically coupled to a membrane-bound compartment whose area, tension, and shape are themselves changing.

The mechanics of this system are already well developed in several directions. Classical tether theory established the force and radius scales of cylindrical lipid membranes under bending and tension, including pressure-force relations for membrane tethers[4-6]. In fission yeast, Lim and colleagues showed that vesicle-like membrane mechanics can account for important aspects of nuclear geometry[7]. Nuclear surface-area management is also biologically consequential: insufficient NE expansion confines and buckles the spindle in *Schizosaccharomyces japonicus*, while experimentally limiting expansion in *S. pombe* can induce spindle buckling and collapse[8]. Lipid regulation and flux provide molecular mechanisms for this expansion[9, 10].

Subsequent models and experiments have made the spindle-NE mechanical coupling increasingly explicit. Continuum models relate spindle- or chromosome-associated loads to nuclear morphology[11, 12], and the apparent flexural response of the NE depends strongly on geometry[13]. The spindle itself is designed to resist compression and buckling[14], while

recent perturbation and ablation studies show reciprocal coupling: increased NE tension bends the spindle, rupturing the envelope relieves spindle compression, and spindle severing relaxes envelope tension[15]. More recent work further supports load-sensitive spindle mechanics and biochemistry[16, 17].

External confinement is likewise not a new concept in mitosis. Animal cells generate hydrostatic pressure and cortical forces to round during mitosis[18]; confined epithelial cells can generate pressures of order hundreds of pascals while rounding or escaping confinement[19]; and fibrous extracellular confinement can reposition and reorient mitotic spindles[20]. These studies establish that confinement can influence mitosis, but they do not determine how an external load would be transmitted through a walled fission-yeast cell to the intranuclear spindle-NE subsystem. Indeed, *S. pombe* turgor pressure is of order 1 MPa[21], underscoring that pressure magnitudes measured in animal cells cannot simply be reinterpreted as yeast environmental or NE loads.

Here I therefore ask a narrower question. If an external confinement pressure is transmitted to the NE, under what reduced mechanical condition does that load become comparable to an adopted spindle-force threshold? The aim is not to introduce a new membrane constitutive law, to claim that confinement is a demonstrated regulator of fission-yeast mitosis, or to explain the evolution of closed mitosis. Instead, I combine established mechanical ingredients into an analytically solvable boundary and ask whether existing parameterizations permit a stable numerical inference. The answer is unexpectedly restrictive: the literature-based illustrative parameterization lies close to a singular boundary where the inferred confinement threshold becomes extremely sensitive to uncertain mechanical calibration.

2. Model and Analytical Framework

2.1. Effective Load and Scope

I represent a locally elongated NE region as a cylindrical effective membrane of radius R and length L. The effective whole-NE bending rigidity is κ and the effective whole-NE tension is σ. An external confinement pressure p_{confine} is assumed to reach the NE only through a transmission factor $T \in [0, 1]$,

$$p_{\mathrm{eff}} = T\, p_{\mathrm{confine}} \quad (1)$$

The parameter T is not measured here; it deliberately collects the unknown mechanical transfer through the cell wall, cortex, cytoplasm, organelles, and nuclear attachments. Thus p_{eff} is a reduced effective load, not a claim that whole-cell confinement acts uniformly or hydrostatically on the NE.

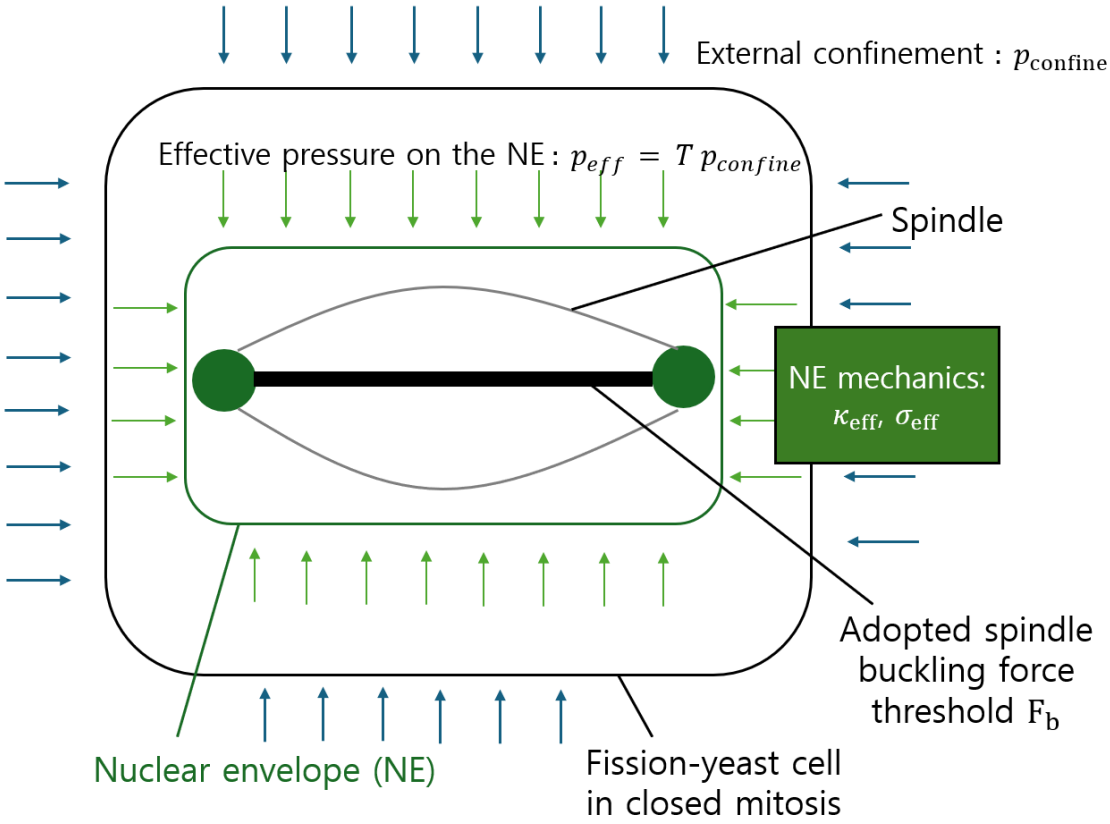


Figure 1. Reduced model of externally transmitted confinement during closed mitosis. External confinement p_{confine} is transmitted to the NE through an unknown fraction T, producing $p_{\mathrm{eff}} = T\, p_{\mathrm{confine}}$. The resulting membrane-load scale is compared with an adopted spindle threshold F_b, yielding the reduced variables $\mu = \frac{F_b}{f_0}$ and $\chi = Tp_{\mathrm{confine}}\sqrt{\frac{\kappa}{2\sigma^3}}$ and the feasibility condition $\chi \geq q^*(\mu)$.

I use F_b as a comparison scale associated with spindle buckling resistance, not as a universal or precisely measured spindle force. At a stationary membrane radius, $f(p_{\mathrm{eff}})$ is the characteristic axial load supported by the reduced membrane model. I use $f(p_{\mathrm{eff}}) = F_b$ as an onset criterion for force-scale comparability, consistent with documented mechanical coupling between the spindle and NE [15,17]. This criterion motivates the feasibility boundary but does not derive detailed force transfer. If only a fraction η of the NE load reaches the spindle, the condition is $\eta f(p_{\mathrm{eff}}) = F_b$, which rescales the effective margin to μ/η; this coupling acts through F_b and μ, rather than being absorbed into the pressure-transmission fraction T.

2.2 Cylindrical Membrane Energy

With the sign convention that positive p_{eff} penalizes enclosed volume, the effective Helfrich energy is

$$F = 2\kappa \int H^2 dA + \sigma A + p_{\mathrm{eff}} V \quad (2)$$

For a cylinder, $H = \frac{1}{(2R)}$, $A = 2\pi RL$, and $V = \pi R^2 L$. The energy per unit length is therefore

$$g(R) \equiv \frac{F}{L} = \frac{\pi\kappa}{R} + 2\pi\sigma R + \pi p_{\mathrm{eff}} R^2 \quad (3)$$

Stationary with respect to radius gives

$$2p_{\mathrm{eff}} R^3 + 2\sigma R^2 - \kappa = 0 \quad (4)$$

At a stationary radius, the axial derivative with respect to L gives the characteristic load

$$f = \frac{\pi\kappa}{R} + 2\pi\sigma R + \pi p_{\text{eff}} R^2 \quad (5)$$

At zero effective pressure, the standard tether radius and force scale are

$$R_D = \sqrt{\frac{\kappa}{2\sigma}},\ f_0 \ = \ 2\pi\sqrt{2\kappa\sigma}, \quad (6)$$

This is consistent with classical membrane-tube mechanics[6].

2.3. Nondimensionalization

Define

$$x = \frac{R}{R_D},\ q = \frac{p_{\text{eff}} R_D}{\sigma},\ \mu = \frac{F_b}{f_0} \quad (7)$$

Equation (4) becomes

$$qx^3 + x^2 - 1 = 0 \quad (8)$$

and Eq. (5) reduces to

$$\frac{f}{f_0} = \frac{1}{4}(\frac{3}{x} + x). \quad (9)$$

3. Results

3.1. The Reduced Model Yields an Exact Dimensionless Feasibility Boundary

The analytical framework above reduces the mechanics to two dimensionless quantities: the intrinsic force margin $\mu = \frac{F_b}{f_0}$ and the pressure coordinate $q = \frac{p_{\text{eff}} R_D}{\sigma}$. The following results are exact consequences of this reduced model; the numerical fission-yeast evaluation is presented separately below.

For $\mu \geq 1$, solving $f = F_b$ on the physical branch $x \leq 1$ gives

$$x^*(\mu) = 2\mu - \sqrt{4\mu^2 - 3}, \quad (10)$$

$$q^*(\mu) = \frac{1 - x^{*2}}{x^{*3}} = \frac{4}{27}[8\mu^3 - 9\mu + (4\mu^2 - 3)^{\frac{3}{2}}]. \quad (11)$$

The corresponding critical effective pressure is

$$p^* = q^*(\mu)\sqrt{\frac{2\sigma^3}{\kappa}}. \quad (12)$$

Finally define a dimensionless transmitted external load

$$\chi = T p_{\text{confine}} \sqrt{\frac{\kappa}{2\sigma^3}}. \quad (13)$$

For $\mu \geq 1$, the reduced threshold condition is therefore

$$\chi \geq q^*(\mu). \quad (14)$$

I refer to Eq. (14) as a universal dimensionless relation in reduced coordinates, not as a parameter-free biological prediction: calculating μ and χ still requires $F_b,\ \kappa,\ \sigma,\ T,\ and\ p_{\mathrm{confine}}$.

For $\mu = 1$, the threshold occurs at zero additional pressure. For $\mu \leq 1$, $f_0 > F_b$ already at $p_{\mathrm{eff}} = 0$; the minimum additional pressure is therefore clamped to $p^* = 0$, while the event "confinement-induced crossing" is not applicable because there is no positive-pressure crossing to induce.

3.2. The Feasibility Boundary is Strictly Increasing and Convex

The exact threshold is strictly increasing and strictly convex for $\mu > 1$:

$$\frac{dq^*}{d\mu} = \frac{4}{x^{*2}} > 0,\ \frac{d^2q^*}{d\mu^2} = \frac{32}{x^*(3-x^{*2})} > 0. \quad (15)$$

Thus, greater intrinsic spindle-to-membrane force margin requires progressively larger transmitted load, rather than a merely linear increase (Fig. 2).

3.3. Threshold Inference Becomes Singularly Sensitive Near the $\mu = 1$ Boundary

Differentiating Eq. (12) gives exact logarithmic elasticities

$$E_{F_b} \equiv \frac{\partial \ln p^*}{\partial \ln F_b} = \frac{3+x^{*2}}{1-x^{*2}}, \quad (16)$$

$$E_\kappa \equiv \frac{\partial \ln p^*}{\partial \ln \kappa} = -\frac{2}{1-x^{*2}}, \quad (17)$$

$$E_\sigma \equiv \frac{\partial \ln p^*}{\partial \ln \sigma} = -\frac{2x^{*2}}{1-x^{*2}}. \quad (18)$$

They satisfy two exact identities,

$$E_{F_b} + E_\kappa + E_\sigma = 1,\ E_\kappa - E_\sigma = -2, \quad (19)$$

All three become large in magnitude as $\mu \to 1^+$ (Fig. 3). Near that boundary, writing $\mu = 1 + \varepsilon$ gives

$$q^* = 4\varepsilon + 8\varepsilon^2 + O(\varepsilon^4), \quad (20)$$

so the positive-pressure threshold emerges linearly from zero. In the opposite limit $\mu \gg 1$,

$$q^* = \frac{64}{27}\mu^3 - \frac{8}{3}\mu + \frac{1}{4\mu} + O(\mu^{-3}). \quad (21)$$

The near- $\mu = 1$ divergence is central to the interpretation below: a numerically small p^* can coexist with extremely poor parameter identifiability.

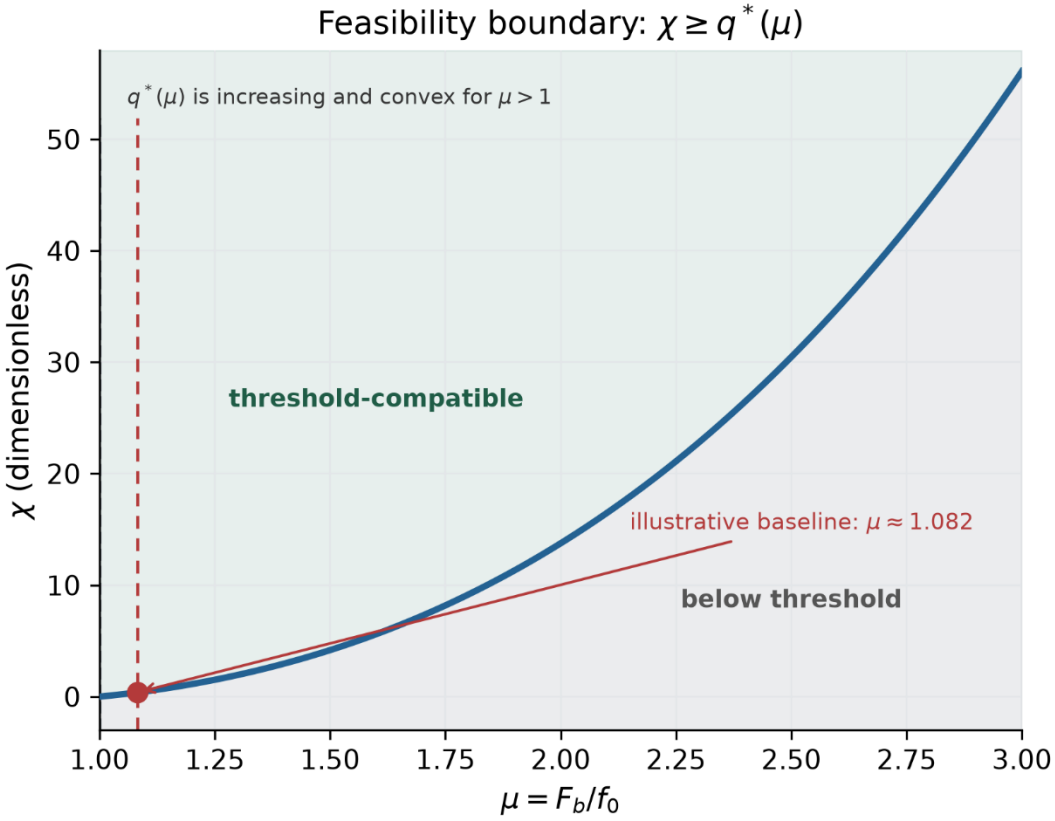


Figure 2. Exact dimensionless threshold. $q^*(\mu)$ increases monotonically and convexly for $\mu > 1$. The marker shows the illustrative Lim-consistent whole-NE parameterization combined with $F_b = 31pN$, giving $\mu \approx 1.082$.

3.4. A Literature-Based Fission-Yeast Parameterization Lies Near the Zero-Pressure Boundary

Because equilibrium shapes are invariant under a uniform rescaling of elastic energy, shape fitting constrains only ratios of the moduli. Lim et al. [7] fit the tension-to-bending ratio, expressed here as $\sigma_{\text{eff}}/\kappa_{\text{eff}} = 65\,\mu\text{m}^{-2}$, and adopt a typical bending modulus $B = 4.00 \times 10^{-19}$ J from Powers et al. [23]. The absolute bending scale is adopted rather than inferred from the shape fit. The corresponding effective tension is the fitted ratio multiplied by the adopted κ_{eff}, so uncertainty in that scale carries σ_{eff} with it. Lim and Huber [22] later wrote the whole-NE energy as $4B_1 \int H^2 dA + 2\sigma_{\text{NE}} A$, with $B_1 = 200\,\text{pN nm}$ and $\sigma_{\text{NE}} = 0.013\,\text{pN/nm}$ per bilayer. Mapping this expression to the single effective-surface convention in Eq. (3) gives the same pair,

$$\kappa_{\text{eff}} = 400pN\ nm,\ \sigma_{\text{eff}} = 0.026\,\tfrac{\text{pN}}{\text{nm}}. \quad (22)$$

Begley et al. [15] tabulate $\kappa = 40\,\text{pN nm}$ and $\sigma = 0.013\,\text{pN/nm}$, which give their reported $f_0 = 6.4\,\text{pN}$. These differ from the main Lim-consistent whole-NE pair used here; the provenance of the tabulated bending modulus remains unresolved and is not treated as a confirmed error. Using the Begley pair gives $\mu \approx 4.84$, $p^* \approx 85\,\text{kPa}$, and $E_{F_b} \approx 3.1$, placing the system farther from the $\mu = 1$ boundary and showing that the near-threshold conclusion depends on the adopted whole-NE convention. Begley et al. also discuss a tension increase of up to 20-fold under cerulenin perturbation [15], unlike the approximately 17% increase sufficient to reach $\mu \leq 1$ under the present baseline.

For the spindle comparison scale, I adopt the illustrative $F_b = 31pN$ calibration used by Begley et al.[15], which builds on the strong length dependence of spindle buckling characterized by Ward et al.[14]. This value is model-calibrated, not a direct universal measurement; later work continues to emphasize heterogeneity and uncertainty in spindle mechanics[16].

With Eq. (22),

$$f_0 = 28.656pN,\ \mu = 1.0818. \quad (23)$$

The positive pressure threshold is then

$$p^* = 112.96Pa. \quad (24)$$

At this same point, however,

$$E_{F_b} = 15.11,\ E_\kappa = -8.05,\ E_\sigma = -6.05. \quad (25)$$

Therefore, 113 Pa should not be read as a measured or robust yeast pressure threshold. It is one fragile evaluation of Eq. (14) near a singular boundary.

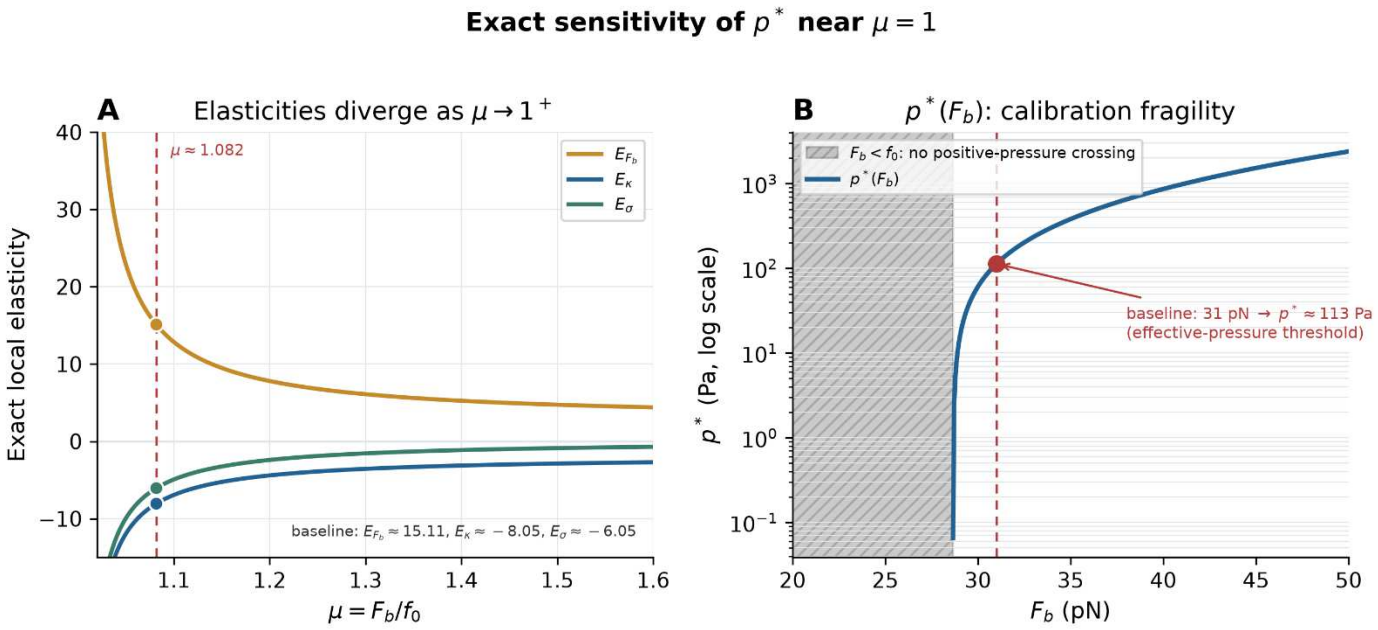


Figure 3. Exact sensitivity of the effective-pressure threshold near the $\mu = 1$ boundary. (A) Exact local elasticities of the inferred threshold pressure p^* with respect to the adopted spindle-force scale F_b, NE bending rigidity κ, and NE tension σ, plotted as functions of $\mu = \frac{F_b}{f_0}$. All three elasticities diverge as $\mu \to 1^+$, indicating that the inferred positive-pressure threshold becomes increasingly sensitive to parameter calibration near the $\mu = 1$ boundary. The illustrative parameterization lies at $\mu \approx 1.082$, with $E_{F_b} \approx 15.11$, $E_\kappa \approx -8.05$, and $E_\sigma \approx -6.05$. **(B)** Dependence of the critical effective pressure p^* on the adopted spindle-force threshold F_b, with κ and σ fixed at the illustrative whole-NE values. For $F_b < f_0 \approx 28.66pN$ (shaded region), the zero-pressure membrane-load scale already exceeds the adopted spindle threshold, so no positive-pressure crossing exists. The illustrative literature-based choice $F_b = 31pN$ lies only slightly above this boundary and gives $p^* \approx 113Pa$. This value is therefore highly sensitive to the adopted force calibration and should be interpreted as an effective-pressure threshold within the reduced model, not as a measured cellular pressure.

3.5 External-to-NE Transmission Remains an Unidentified Control Parameter

For a given whole-cell confinement pressure and $\mu > 1$, the required transmission fraction is

$$T_{\text{crit}} = \frac{p^*}{p_{\text{confine}}}, \quad (26)$$

Under the illustrative baseline, $T_{\text{crit}} \approx 0.664$ at 170 Pa and $T_{\text{crit}} \approx 0.127$ at 890 Pa. Figure 4 shows this mapping over a range of adopted spindle thresholds.

The 170–890 Pa band shown in the figure comes from confined MDCK epithelial cells [19]; it is included solely as a contextual example of a mitotic pressure scale in an unrelated animal-cell system. It is not an estimate of pressure acting on *S. pombe*. Fission yeast has a cell wall and a turgor pressure of approximately 1 MPa [21]. Consequently, the transmission fraction T is a genuine missing mechanical quantity rather than a cosmetic correction factor.

3.6 Deterministic Stress Test Reveals Regime Switching

As a first, distribution-free stress test, I varied κ, σ, and F_b independently by $\pm 5\%$, $\pm 10\%$, and $\pm 20\%$. These are deterministic stress tests, not confidence intervals. Four of 21 rows cross into the $\mu \leq 1$ regime: $\kappa + 20\%$, $\sigma + 20\%$, $F_b - 10\%$, and $F_b - 20\%$. Among the remaining positive-pressure cases, p^* spans a broad range but remains below 890 Pa in this particular OAT grid, reaching approximately 573 Pa for $F_b + 20\%$. The key observation is not accessibility relative to the animal-cell contextual band; it is the regime change itself. Small independent perturbations can eliminate the positive pressure crossing because the baseline is so close to $\mu = 1$ (Supplementary Fig. S1).

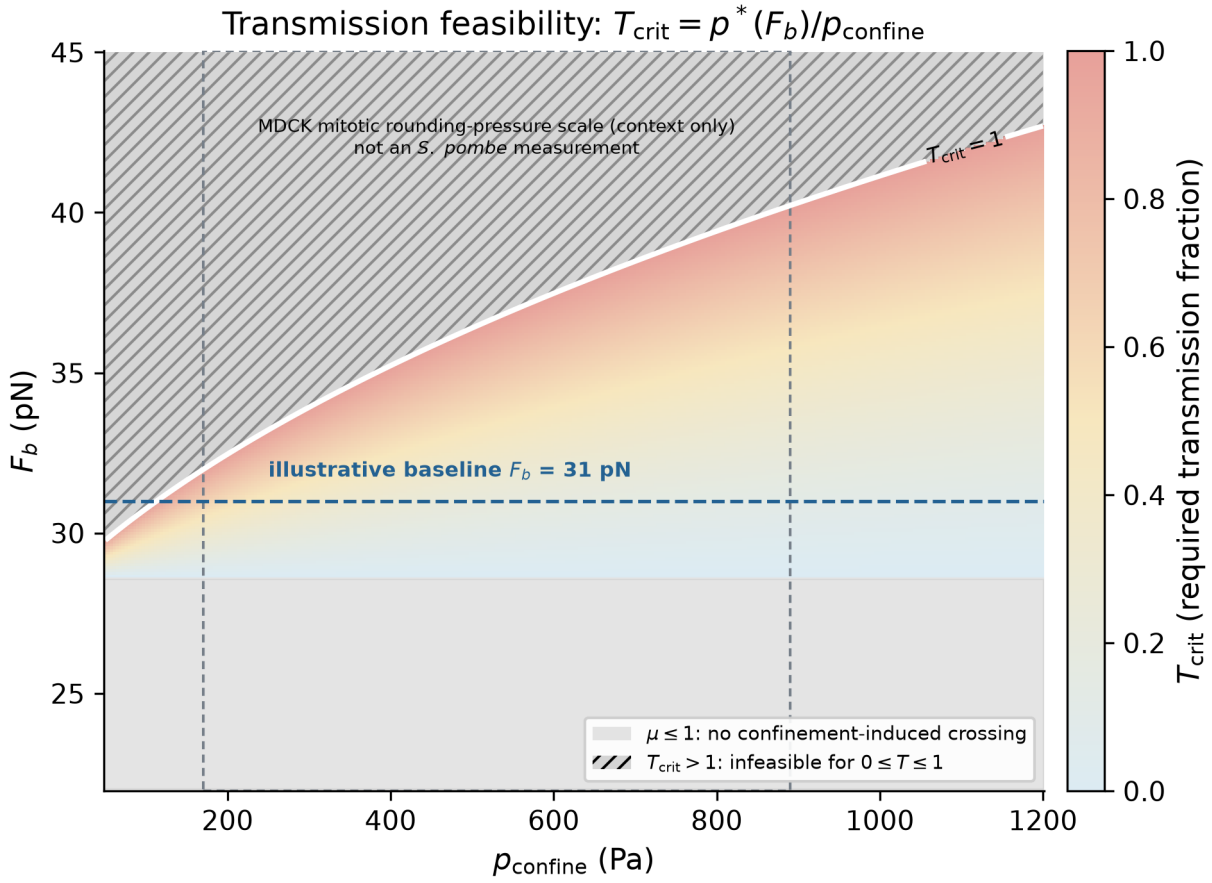


Figure 4. Transmission feasibility map. Color indicates the required transmission fraction $T_{\text{crit}} = \frac{p^*(F_b)}{p_{\text{confine}}}$. The upper hatched region has $T_{\text{crit}} > 1$ and is therefore inaccessible for $0 < T < 1$, whereas the lower shaded region has $\mu \leq 1$, for which no positive-pressure confinement-induced crossing exists. The dashed line marks the illustrative $F_b = 31pN$ calibration. The 170-890 Pa MDCK range from Sorce et al. is shown for context only.

3.7. Assumption-Dependent Scenario Propagation Shows Frequent Regime Switching

For each relative half-width $\delta \in \{0.05, 0.10, 0.20\}$, I generated 10^6 draws with random seed 20261101. In the independent scenario, κ_{eff}, σ_{eff}, and F_b were sampled independently from uniform distributions centered on their illustrative values. In the ratio-fixed scenario, κ_{eff} and F_b were sampled independently and σ_{eff} was set to $(\sigma_{\text{eff}}/\kappa_{\text{eff}})_{\text{fit}}\kappa_{\text{eff}}$, preserving the fitted ratio. For each draw, p^* was calculated from Eqs. (11)–(12), with the stated $\mu \leq 1$ regime semantics. Monte Carlo standard errors for the positive-crossing fractions were below 0.05 percentage points. The fitted-ratio scenario is the primary comparison because it preserves the parameter provenance in Section 3.4.

Table 24: Scenario-based propagation under fitted-ratio-preserving (primary) and independent perturbations. Pressure quantiles are conditional on $\mu > 1$; exceedance probabilities use all draws.

	$P(\mu > 1)$ (%)		Conditional median p^* (Pa)		Conditional 97.5th percentile p^* (Pa)		$P(p^* > 890\,\text{Pa})$ (%)	
δ	Ratio fixed	Independent	Ratio fixed	Independent	Ratio fixed	Independent	Ratio fixed	Independent
5%	97.7	99.3	115	114	260	238	0.0	0.0
10%	81.6	85.1	146	140	458	405	0.0	0.0
20%	67.7	69.5	246	235	1,048	902	3.9	1.9

Preserving the fitted ratio produces more regime switching and a wider upper tail than independent perturbation. Both effects follow from the sign structure of the model. Because κ_{eff} and σ_{eff} enter μ with the same sign,

$$\ln \mu = \ln F_b - \tfrac{1}{2} \ln \kappa_{\text{eff}} - \tfrac{1}{2} \ln \sigma_{\text{eff}} + \text{const}, \tag{1}$$

co-varying them widens $\ln \mu$: for half-width δ, $s \equiv \text{sd}(\ln \mu) \simeq \delta/\sqrt{2}$ (independent) and $\delta\sqrt{2/3}$ (ratio fixed). Likewise, the local membrane contribution to $\ln p^*$ scales with $\sqrt{E_\kappa^2 + E_\sigma^2} \approx 10.1$ under independent variation but with $|E_\kappa + E_\sigma| = |1 - E_{F_b}| \approx 14.1$ (Eq. 19) when the ratio is fixed. Uncertainty in the fitted ratio itself would add a variance term to $\ln \mu$ if propagated as an independent source; the independent κ–σ scenario is therefore not a conservative bound.

A normal approximation provides an analytic check for both scenarios:

$$P(\mu > 1) \simeq \Phi\left(\frac{\ln \mu_0}{s}\right), \qquad \ln \mu_0 \simeq 0.079, \tag{2}$$

giving 98.7%, 86.7%, and 71.1% (independent), and 97.3%, 83.2%, and 68.5% (ratio fixed), within two percentage points of the Monte Carlo values. The baseline margin equals one standard deviation of $\ln \mu$ at $\delta \simeq 11\%$ (independent) or $\simeq 9.6\%$ (ratio fixed).

Conditioning on $\mu > 1$ excludes draws in the $\mu \leq 1$ regime, while the strict convexity of $q^*(\mu)$ (Eq. 15) expands the upper tail. At $\delta = 20\%$, 1.9% of independent draws and 3.9% of ratio-fixed draws have $p^* > 890$ Pa. At the contextual pressure of 890 Pa, these draws would require $T_{\text{crit}} > 1$; even full transmission would not reach the threshold, corresponding to the hatched infeasible region of Fig. 4.

Scope of the scenario analysis. These probabilities are conditional on the specified perturbation models; they are not empirical probabilities for biological parameters. The fitted $\sigma_{\text{eff}}/\kappa_{\text{eff}}$ ratio and the weak constraint on the absolute κ_{eff} scale motivate the ratio-fixed scenario, while the independent scenario is retained only as a comparison. Neither scenario substitutes for measured parameter distributions.

4. Discussion

The main contribution of this work is a reduced analytical framework that connects externally applied confinement to the spindle-nuclear-envelope (NE) subsystem during closed mitosis. By introducing an external-to-NE transmission fraction T, the problem is reduced to two dimensionless control variables, $\mu = \frac{F_b}{f_0}$ and $\chi = T p_{\text{confine}} \sqrt{\frac{\kappa}{2\sigma^3}}$, with the exact feasibility boundary $\chi = q^*(\mu)$. The underlying ingredients—membrane-tube mechanics, fission-yeast NE mechanics, spindle buckling, reciprocal spindle-NE coupling, and confinement effects on mitosis—are established[6, 7, 14, 15, 19]. The novelty here is therefore not a new constitutive law, but the explicit connection of external confinement to the closed-mitotic spindle-NE force comparison and its reduction to a compact dimensionless criterion.

The reduction also reveals that the numerical threshold is much less robust than a single value such as $p^* \approx 113$ Pa might suggest. For the illustrative *S. pombe* parameterization, $\mu \approx 1.082$ lies close to the $\mu = 1$ boundary. In particular, $E_{F_b} = \partial \ln p^* / \partial \ln F_b \approx 15.1$, so a small fractional change in the adopted spindle-force scale produces a much larger fractional change in p^*. Under $\pm 10\%$ perturbations, approximately 15% of independent draws and 18% of ratio-fixed draws fall in the $\mu \leq 1$ regime; under $\pm 20\%$, the corresponding fractions are approximately 31% and 32%. At $\pm 20\%$, 1.9% of independent draws and 3.9% of ratio-fixed draws also exceed 890 Pa, whereas no row in the deterministic OAT grid exceeds this contextual bound. The 890 Pa value remains an animal-cell reference and does not establish accessibility when T is unknown. The more general result is therefore the geometry of the reduced feasibility boundary and the near-boundary sensitivity it exposes, rather than the specific pressure obtained from one parameter set. These sensitivities also set useful calibration targets: a one-sided 95% statement that the baseline lies above the crossing boundary requires force-margin uncertainty $s = \text{sd}(\ln \mu) \lesssim \ln \mu_0 / 1.645 \approx 4.8\%$, while keeping inferred p^* within a factor of two locally requires relative precision in F_b of about $\ln 2 / E_{F_b} \approx 4.6\%$. These are model-based precision targets, not estimates of current measurement error.

A quantitative biological prediction will require better calibration of the quantities that connect the reduced theory to the cell. The adopted F_b is not an independently measured universal spindle threshold[15, 16], the external-to-NE transmission fraction T is unknown, and the characteristic membrane-load scale $f(p_{\text{eff}})$ should not be interpreted as a direct measurement of the compressive force delivered to the spindle poles. The model is also intentionally static and local, and does not resolve full nuclear geometry, membrane supply, spindle dynamics, heterogeneous force transmission, cortex or cell-wall mechanics, or local NE remodeling. These limitations suggest a clear experimental path: direct measurements of spindle buckling force, NE mechanical response, and spindle deformation under controlled external confinement would

allow the criterion $\chi \geq q^*(\mu)$ to be tested prospectively rather than evaluated only through literature-based parameter estimates.

The present analysis should therefore be interpreted as a feasibility framework rather than as evidence that confinement caused or selected closed mitosis. Mitotic strategies span intermediate states[1, 2], and other constraints—including membrane availability and lipid regulation[8-10], NE remodeling[3], and life-cycle architecture[24]—are already supported experimentally. External confinement is better viewed as one possible mechanical modifier of a closed-mitotic system. The value of the reduced model is that it makes this narrower hypothesis quantitative, identifies where inference becomes unstable, and specifies which future measurements would be most informative.

5. Reproducibility and Code Availability

All analytical expressions, parameter definitions, numerical cross-checks, deterministic stress tests, and figure-generation scripts are available at: https://github.com/HyeonjeYang/closed-mitosis-confinement-mechanics

The repository uses a convention-consistent whole-NE parameterization and cross-checks the closed-form solution against numerical solutions of the original stationarity and force equations. Independent and ratio-fixed scenario propagations are reproducible with `scripts/statistical_robustness.py`; summaries are in `results/robustness_uniform_scenarios.csv`. This study contains no new experimental data.

Data Availability Statement

This study contains no new experimental data. All analytical and numerical materials required to reproduce the results are available in the public GitHub repository listed above.

AI Use Disclosure

OpenAI ChatGPT and Anthropic Claude Code were used for coding and documentation assistance. All scientific interpretation, code review, and final validation were performed by the author.

6. References

[1] C. P. De Souza and S. A. Osmani, "Mitosis, not just open or closed," *Eukaryot Cell,* vol. 6, no. 9, pp. 1521–7, Sep 2007, doi: 10.1128/EC.00178-07.

[2] S. Sazer, M. Lynch, and D. Needleman, "Deciphering the evolutionary history of open and closed mitosis," *Curr Biol,* vol. 24, no. 22, pp. R1099–103, Nov 17 2014, doi: 10.1016/j.cub.2014.10.011.

[3] G. Dey *et al.*, "Closed mitosis requires local disassembly of the nuclear envelope," *Nature,* vol. 585, no. 7823, pp. 119–123, Sep 2020, doi: 10.1038/s41586-020-2648-3.

[4] R. E. Waugh and R. M. Hochmuth, "Mechanical equilibrium of thick, hollow, liquid membrane cylinders," *Biophys J,* vol. 52, no. 3, pp. 391–400, Sep 1987, doi: 10.1016/S0006-3495(87)83227-7.

[5] L. Bo and R. E. Waugh, "Determination of bilayer membrane bending stiffness by tether formation from giant, thin-walled vesicles," *Biophys J,* vol. 55, no. 3, pp. 509–17, Mar 1989, doi: 10.1016/S0006-3495(89)82844-9.

[6] I. Derenyi, F. Julicher, and J. Prost, "Formation and interaction of membrane tubes," *Phys Rev Lett,* vol. 88, no. 23, p. 238101, Jun 10 2002, doi: 10.1103/PhysRevLett.88.238101.

[7] H. W. G. Lim, G. Huber, Y. Torii, A. Hirata, J. Miller, and S. Sazer, "Vesicle-like biomechanics governs important aspects of nuclear geometry in fission yeast," *PLoS One,* vol. 2, no. 9, p. e948, Sep 26 2007, doi: 10.1371/journal.pone.0000948.

[8] C. Yam, Y. He, D. Zhang, K. H. Chiam, and S. Oliferenko, "Divergent strategies for controlling the nuclear membrane satisfy geometric constraints during nuclear division," *Curr Biol,* vol. 21, no. 15, pp. 1314–9, Aug 9 2011, doi: 10.1016/j.cub.2011.06.052.

[9] M. Makarova, Y. Gu, J. S. Chen, J. R. Beckley, K. L. Gould, and S. Oliferenko, "Temporal Regulation of Lipin Activity Diverged to Account for Differences in Mitotic Programs," *Curr Biol,* vol. 26, no. 2, pp. 237–243, Jan 25 2016, doi: 10.1016/j.cub.2015.11.061.

[10] S. Foo, A. Cazenave-Gassiot, M. R. Wenk, and S. Oliferenko, "Diacylglycerol at the inner nuclear membrane fuels nuclear envelope expansion in closed mitosis," *J Cell Sci,* vol. 136, no. 3, Feb 1 2023, doi: 10.1242/jcs.260568.

[11] Q. Zhu, F. Zheng, A. P. Liu, J. Qian, C. Fu, and Y. Lin, "Shape Transformation of the Nuclear Envelope during Closed Mitosis," *Biophys J,* vol. 111, no. 10, pp. 2309–2316, Nov 15 2016, doi: 10.1016/j.bpj.2016.10.004.

[12] C. Fang *et al.*, "A model for bridging microtubule dynamics with nuclear envelope shape evolution during closed mitosis," *Journal of the Mechanics and Physics of Solids,* vol. 144, 2020, doi: 10.1016/j.jmps.2020.104116.

[13] A. Agrawal and T. P. Lele, "Geometry of the nuclear envelope determines its flexural stiffness," *Mol Biol Cell,* vol. 31, no. 16, pp. 1815–1821, Jul 21 2020, doi: 10.1091/mbc.E20-02-0163.

[14] J. J. Ward, H. Roque, C. Antony, and F. Nedelec, "Mechanical design principles of a mitotic spindle," *Elife,* vol. 3, p. e03398, Dec 18 2014, doi: 10.7554/eLife.03398.

[15] M. A. Begley *et al.*, "Mechanical Coupling With the Nuclear Envelope Shapes the Schizosaccharomyces pombe Mitotic Spindle," *Cytoskeleton (Hoboken),* vol. 83, no. 1, pp. 40–52, Jan 2026, doi: 10.1002/cm.22035.

[16] P. Real-Calderon, T. G. Fai, R. R. Daga, J. Lemiere, and F. Chang, "Analyses of bent spindles reveal the mechanics of anaphase B in fission yeast," *Mol Biol Cell,* vol. 37, no. 4, p. ar38, Apr 1 2026, doi: 10.1091/mbc.E25-11-0556.

[17] T. Mahoney, C. Needham, R. Hakeem, M. Begley, C. P. Medina, and M. W. Elting, "Compressive force from the nuclear envelope in dividing S. pombe alters binding of mitotic spindle proteins and regulates microtubule dynamics," bioRxiv, Aug. 26, 2026, doi: 10.64898/2026.01.15.699759.

[18] M. P. Stewart, J. Helenius, Y. Toyoda, S. P. Ramanathan, D. J. Muller, and A. A. Hyman, "Hydrostatic pressure and the actomyosin cortex drive mitotic cell rounding," *Nature,* vol. 469, no. 7329, pp. 226–30, Jan 13 2011, doi: 10.1038/nature09642.

[19] B. Sorce *et al.*, "Mitotic cells contract actomyosin cortex and generate pressure to round against or escape epithelial confinement," *Nat Commun,* vol. 6, p. 8872, Nov 25 2015, doi: 10.1038/ncomms9872.

[20] A. Sarkar *et al.*, "Confinement in fibrous environments positions and orients mitotic spindles," *PNAS Nexus,* vol. 4, no. 7, p. pgaf201, Jul 2025, doi: 10.1093/pnasnexus/pgaf201.

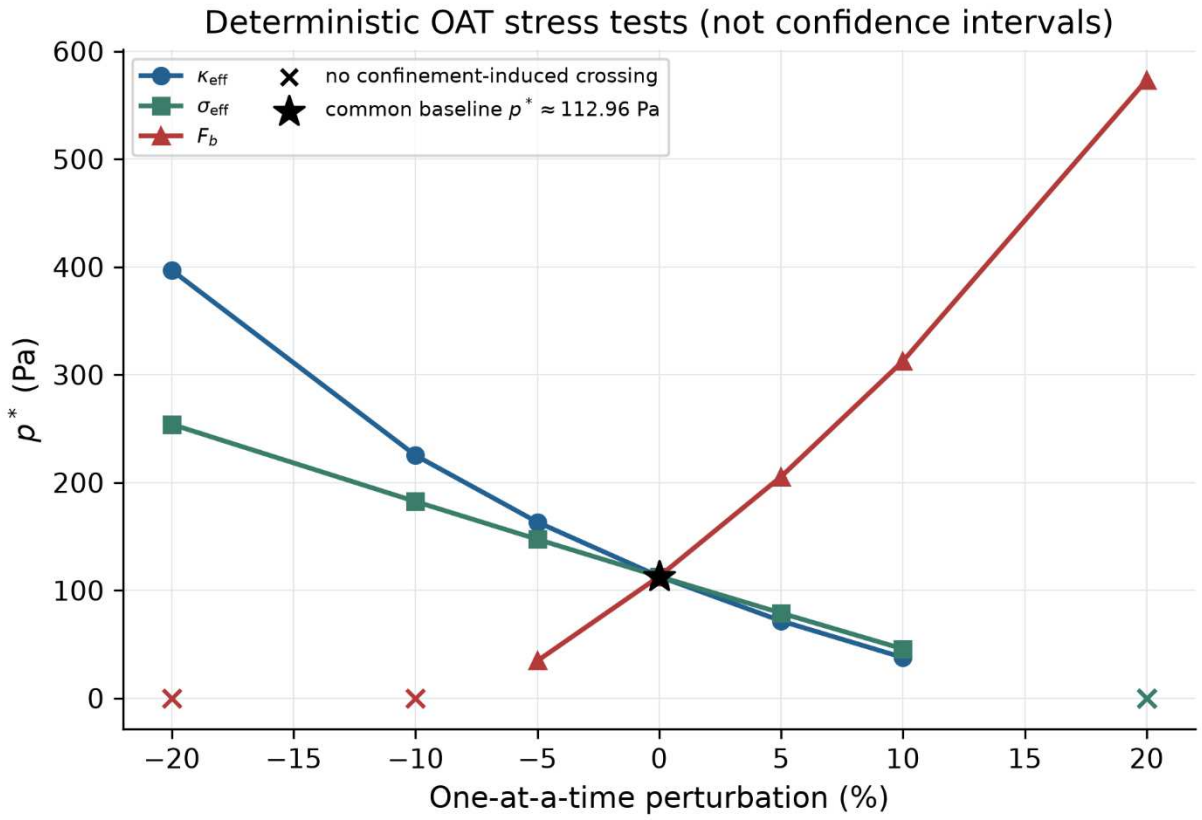
[21] J. Lemiere and F. Chang, "Quantifying turgor pressure in budding and fission yeasts based upon osmotic properties," *Mol Biol Cell,* vol. 34, no. 13, p. ar133, Dec 1 2023, doi: 10.1091/mbc.E23-06-0215.

[22] G. H. Lim and G. Huber, "The tethered infinitesimal tori and spheres algorithm: a versatile calculator for axisymmetric problems in equilibrium membrane mechanics," *Biophys J,* vol. 96, no. 6, pp. 2064–81, Mar 18 2009, doi: 10.1016/j.bpj.2008.10.074.

[23] T. R. Powers, G. Huber, and R. E. Goldstein, “Fluid-membrane tethers: Minimal surfaces and elastic boundary layers, *Phys. Rev. E*, vol. 65, p. 041901, 2002, doi: 10.1103/PhysRevE.65.041901.

[24] H. Shah *et al.*, "Life-cycle-coupled evolution of mitosis in close relatives of animals," *Nature,* vol. 630, no. 8015, pp. 116–122, Jun 2024, doi: 10.1038/s41586-024-07430-z.

Supplementary



Supplementary Figure S1. Deterministic one-at-a-time sensitivity analysis of the inferred pressure threshold. Each of κ_{eff}, σ_{eff}, and F_b was perturbed independently around the illustrative baseline while the other parameters were held fixed. The common baseline is $p^* \approx 112.96 Pa$. Crosses denote perturbations for which $\mu \leq 1$, so no confinement-induced positive-pressure crossing exists. These perturbations are deterministic stress tests and should not be interpreted as confidence intervals.